crystals

MDPI

Article

Hydrothermal Synthesis and Crystal Structure of Vesuvianite Compounds, $Ca_{19}Al_{13}Si_{18}O_{71}(OH)_7$ and $Sr_{19}Fe_{12}Ge_{19}O_{72}(OH)_6$

Megan M. Smart, Cheryl A. Moore, Colin D. McMillen * and Joseph W. Kolis *

Department of Chemistry, Center for Optical Materials Science and Engineering Technologies (COMSET), Clemson University, Clemson, SC 29634, USA; mmsmart@g.clemson.edu (M.M.S.); orionnebula66@yahoo.com (C.A.M.)

* Correspondence: cmcmill@clemson.edu (C.D.M.); kjoseph@clemson.edu (J.W.K.)

Abstract: New compositions of synthetic vesuvianite were investigated using hydrothermal synthesis. High quality single crystals with the formula $Ca_{19}Al_{13}Si_{18}O_{71}(OH)_7$ (**I**) having the vesuvianite-type structure were crystallized during a high temperature hydrothermal growth reaction. Starting materials of Al_2O_3 and $CaSiO_3$ reacted at 670 °C and 2 kbar in 0.5 M aqueous alkali hydroxide mineralizer to form single crystals up to 0.25 mm per edge. Similar reactions employing SrO, Fe_2O_3, and GeO_2 reacting at 580 °C and 2 kbar in 6 M aqueous alkali hydroxide mineralizers led to the formation of the analogous $Sr_{19}Fe_{12}Ge_{19}O_{72}(OH)_6$ (**II**). These crystals were obtained in sizes up to 0.5 mm per edge. The structures of both compounds were refined in space group *P*4/*nnc* after careful evaluation of the diffraction data and subsequent test refinements. Elemental analysis indicated only the presence of Ca^{2+}, Al^{3+}, and Si^{4+} cations in **I** and only the presence of Sr^{2+}, Fe^{3+}, and Ge^{4+} cations in **II**, representing synthetic vesuvianite comprising the minimum number of unique cations. The use of larger cations than are typically found in natural vesuvianite, such as Sr^{2+}, Fe^{3+}, and Ge^{4+}, resulted in an expanded crystalline lattice and extended the vesuvianite analogs to include an increasing variety of elements.

Keywords: vesuvianite; hydrothermal; crystal structure; synthesis; crystal growth

Citation: Smart, M.M.; Moore, C.A.; McMillen, C.D.; Kolis, J.W. Hydrothermal Synthesis and Crystal Structure of Vesuvianite Compounds, $Ca_{19}Al_{13}Si_{18}O_{71}(OH)_7$ and $Sr_{19}Fe_{12}Ge_{19}O_{72}(OH)_6$. *Crystals* **2023**, *13*, 1257. https://doi.org/10.3390/cryst13081257

Academic Editor: Francesco Capitelli

Received: 24 July 2023
Revised: 10 August 2023
Accepted: 11 August 2023
Published: 15 August 2023

1. Introduction

Vesuvianite is one of the most architecturally ambiguous structure types known [1–4]. It is a fairly common mineral isolated all over the world, but it has considerable structural complexity due to its tendency to accommodate an enormously wide range of elements within its various lattice sites [5–10]. As an indicator of its complicated behavior, there have been no less than three complete PhD theses dedicated to its structural determination [11–13]. The compound has the generic formula $X_{19}Y_{13}Z_{18}O_{68}W_{10}$, where *X*, *Y*, and *Z* are cation sites and *W* sites are mono- or dianion sites. The *X* sites are generally eight to nine coordinates, while the *Y* sites are generally approximately six coordinate octahedral sites; the *Z* sites are four coordinate tetrahedral sites. While there is an enormous range of atoms and ionic charges that are known to substitute into the basic framework, the bulk of the substitutions occur on the *X* and *Y* sites, with the *Z* site mostly remaining tetrahedral silicon in the vast majority of natural samples. The *W* site can be occupied by monovalent (OH^-, F^-) anions, though it can also have some divalent oxide anion occupancy, allowing for variation of the number of hydrogen ions on this site providing another flexible mode to accommodate charge balance. Within the lattice, there are three unique crystallographic sites for *X*, *Y*, and *Z*, each with different site symmetry and occupancy number; these are combined with 10 unique oxygen sites and the additional monovalent anion site.

The selection of coordination environments in vesuvianite is reminiscent of garnet and, indeed, the materials have a number of similarities. The primary difference is that vesuvianite is a more open structure because it contains channels down one axis that are

occupied in a disordered fashion by various amounts of additional *X* and *Y* ions. The presence of these channels lowers the symmetry to tetragonal, with the most common space group being *P*4/*nnc*. The variation of the disorder pattern along the channels and the variation of ions in the channels provide an extensive array of structural possibilities; a number of other space groups have been identified, such as *P*4/*n* and acentric *P*4*nc* [14–17]. These lower symmetry tetragonal structures are based on the ordering pattern of the *X* and *Y* ions within the columns and the relationship of the columns with each in the lattice. All of these variabilities and chemical and structural degrees of freedom make it easy to see why this structure type has such a rich structural history.

To our knowledge a "parent" vesuvianite phase (analogous to grossular garnet) with the formula $Ca_{19}Al_{13}Si_{18}O_{71}(OH)_7$ has not been reported from either natural or synthetic conditions. Typically, the Ca and Al sites are heavily substituted with a wide range of other ions, notably iron and magnesium. We have previously had good success in employing high temperature hydrothermal conditions (500–700 °C) in preparing a wide range of mineralogically inspired materials as high quality single crystals [18–21]. In our attempts to prepare grossular single crystals (garnet, $Ca_3Al_2Si_3O_{12}$) in high temperature hydrothermal systems, we sometimes observed vesuvianite accompanied by the grossular formation. It is not surprising that vesuvianite crystals occurred in similar synthetic environment as grossular, as, in many cases, vesuvianite occurs commonly with grossular in natural systems as well. The two phases, grossular and vesuvianite, have long been joined together as structurally and chemically similar relatives. In fact, the original study of vesuvianite called attention to this relationship [22].

There have been several previous attempts to synthesize vesuvianite under controlled conditions, mostly using hydrothermal methods. These attempts were reviewed by Ito and Arem [3]. In particular, some syntheses of Mg-free vesuvianite summarized in that work led to nebulous results that deviate from today's accepted formula for vesuvianite and could not be structurally characterized in detail. Those results on the Mg-free system could not be reproduced during a thorough synthetic effort, where only grossular was reported [3]. Those researchers did succeed in synthesizing a powder identified as $Ca_{19}Mg_4Al_{10}Si_{17}O_{68}(OH)_8 \cdot nH_2O$ and characterized it as a vesuvianite using powder X-ray diffraction and electron microprobe analysis. This previous work was done at sufficiently high temperatures (300–700 °C), but usually contained Mg^{2+} in the starting material and did not have very high base concentrations in the mineralizer; these factors may account for their failure to obtain high quality single crystals of $Ca_{19}Al_{13}Si_{18}O_{71}(OH)_7$.

We were also curious if the vesuvianite structure type could be expanded into a new phase space through the substitution of the larger tetrahedral Ge^{4+} ion for Si^{4+}. We have recently been examining the role of germanate as a building block in transition metal oxides and have observed some complex structural chemistry [23,24]. In the present case, we found that the larger germanate can accommodate the larger Fe^{3+} ion in the trivalent Al^{3+} sites, as well as the larger Sr^{2+} ion in the Ca^{2+} sites. Under the appropriate conditions, we can isolate well-formed single crystals (pure $Sr_{19}Fe_{12}Ge_{19}O_{72}(OH)_6$) in an essentially quantitative yield. Given that it has the same structure as the iron-free $Ca_{19}Al_{13}Si_{18}O_{71}(OH)_7$, we think that it provides an opportunity to study these interesting end members of a fascinating and complex material. Furthermore, the growth of Fe^{3+}-containing materials lays the groundwork for subsequent magnetic studies of this phase. The detailed structural and crystallographic examinations of these two end-member formulations are reported here.

2. Materials and Methods

2.1. Synthesis

Single crystals of the vesuvianite compounds were obtained from hydrothermal reactions performed at 670 °C and 580 °C, for $Ca_{19}Al_{13}Si_{18}O_{71}(OH)_7$, **I**, and $Sr_{19}Fe_{12}Ge_{19}O_{72}(OH)_6$, **II**, respectively. For **I**, starting materials consisting of $CaSiO_3$ and Al_2O_3 were mixed in a 1:1 molar ratio and loaded into silver reaction ampoules. Aqueous sodium hydroxide mineralizer (0.5 M, 0.4 mL) was added to the ampoules, which were subsequently weld-

sealed. For **II**, the synthesis used SrO, Fe_2O_3, and GeO_2 in a 3:1:3 molar ratio, with 0.4 mL of 6 M KOH as the mineralizer. It was found that **II** could also be successfully synthesized with FeO as the transition metal source and with NaOH, RbOH, and CsOH mineralizers at 3 M and 6 M concentrations. The ampoules were placed in a Tuttle cold seal autoclave; the autoclave was filled with deionized water to provide a positive counter pressure. The autoclave was outfitted with external band heaters and heated to the target temperature, where it was held for five days for **I** and seven days for **II**, generating approximately 2 kbar pressure. The autoclave was then cooled to room temperature over 12 h and the products were harvested from the ampoules. Two morphologies of colorless crystals were observed in approximately equal quantities for the first set of reactions: elongated prismatic crystals corresponding to **I** and rhombic dodecahedra corresponding to synthetic grossular garnet. In contrast, the synthesis for **II** produced elongated prismatic crystals and large blocks of a very dark red color, with PXRD patterns showing phase-pure vesuvianite as the sole reaction product.

2.2. Single Crystal X-ray Diffraction

Single crystal X-ray diffraction of a colorless columnar crystal was performed at room temperature for colorless **I** and a dark red block crystal at 105(2) K for **II,** using a Bruker D8 Venture diffractometer. The data were collected using phi and omega scans (0.50° oscillations) with a Mo Kα (λ = 0.71073 Å) microfocus source and Photon 100 detector. Data were processed using the SAINT software program and corrected for absorption using the SADABS multi-scan technique, both within the Apex3 suite [25]. The structures were solved by direct methods and subsequently refined by full matrix least squares on F^2 using the SHELXTL software package [26]. Space group symmetry of *P*4/*nnc* was determined based on the systematic absences for both compounds, though further analysis was also performed in *P*4*nc* and *P*4/*n*. All non-hydrogen atoms were refined anisotropically. Atoms Ca4 and Al1 were refined as half-occupied, based on geometric constraints in **I** (typical of the vesuvianite structure type). For **II**, the refinement of atoms Sr4a/Sr4b and Ge4a/Ge4b were first performed through a combination of the SUMP and FVAR commands in SHELX and were then fixed to the nearest 1/10th site occupancy for an overall 50:50 Sr:Ge ratio across the four sites. Hydrogen atoms corresponding to the OH groups in the structure were identified from the difference electron density map and distance fixing restraints were used to maintain appropriate O-H contact distances. The structure solution for **I** was refined to a final R1 of 0.0337 and wR2 of 0.0782, based on the observed data ($I > 2\sigma I$), with the refinements resulting in a final R1 of 0.0461 and a wR2 of 0.0694 for **II.** Complete refinement details for both compounds are summarized in Table 1. CSD 2284129-2284130 contains the supplementary crystallographic data for this paper. These data can be obtained free of charge via http://www.ccdc.cam.ac.uk/conts/retrieving.html (or from the CCDC, 12 Union Road, Cambridge CB2 1EZ, UK; Fax: +44 1223 336033; E-mail: deposit@ccdc.cam.ac.uk).

Table 1. Crystallographic data and refinement details for **I** and **II**.

	I	**II**
Empirical Formula	$Ca_{19}Al_{13}Si_{18}O_{78}H_7$	$Sr_{19}Fe_{12}Ge_{19}O_{78}H_6$
F. W. (g/mol)	2872.94	4968.24
Temperature (K)	296(2)	105(2)
Crystal System	Tetragonal	Tetragonal
Space Group	*P4/nnc* (no. 126)	*P4/nnc* (no. 126)
a (Å)	15.5429(16)	16.4498(8)
c (Å)	11.8210(12)	12.4779(6)
Volume (Å^3)	2855.7(7)	3376.5(4)
Z	2	2
D(calcd) (mg/m^3)	3.341	4.887
Wavelength (Å)	0.71073	0.71073

Table 1. *Cont.*

	I	**II**
μ, mm^{-1}	2.494	25.793
F(000)	2864	4544
Crystal Size (mm)	0.055 × 0.061 × 0.101	0.114 × 0.085 × 0.055
θ range,°	2.621 to 30.530	3.215 to 30.469
Reflections Collected	2188	2579
Independent Reflections	1958	2149
R indices (I > 2σ(I))	R_1 = 0.0337 [a] wR_2 = 0.0782 [b]	R_1 = 0.0461 [a] wR_2 = 0.0694 [b]
R indices (all data)	R_1 = 0.0404 [a] wR_2 = 0.0803 [b]	R_1 = 0.0624 [a] wR_2 = 0.0727 [b]
Goodness-of-fit on F^2	1.228	1.164

[a] $R_1 = ||F_o| - [F_c||/|F_o|$. [b] $wR_2 = \{[w(F_o^2 - F_c^2)^2]/[wF_o^2]^2\}^{1/2}$.

2.3. Additional Characterization

Elemental analysis of the crystalline products was performed using energy dispersive X-ray analysis (EDX). Samples of the colorless and dark red elongated prismatic crystals and rhombic dodecahedra were mounted on carbon tape and loaded into a Hitachi S-3400N scanning electron microscope equipped with an Oxford INCA EDX detector. An accelerating voltage of 20 kV was used and multiple data points were inspected on multiple crystals. At all analysis points, only the presence of Ca, Al, Si, and O was observed for the colorless elongated prismatic vesuvianite **I** and only Sr, Fe, Ge, and O for the dark red vesuvianite **II**.

Bulk reaction products were evaluated by powder X-ray diffraction using a Rigaku Ultima IV diffractometer. Well-ground samples were analyzed in Bragg–Brentano geometry using Cu Kα (λ = 1.5406 Å) radiation. Data were collected from 15 to 65 degrees in 2-theta at a rate of 1 degree per minute. Analysis of the resulting patterns for **I** confirmed the presence of two products corresponding to the vesuvianite and garnet structure types, with the patterns for **II** corresponding only to the vesuvianite-type phase.

Single crystal Raman scattering measurements for **I** were performed using an Olympus IX71 inverted microscope with a 20× objective lens coupled to a TRIAX 552 spectrometer equipped with a thermoelectrically cooled CCD detector (Andor Technology, Model DU420A-BV) operating at −60 °C. An argon ion laser (Innova 100, Coherent) was used to excite the Raman signal with 514.5 nm light in a 180° backscattering geometry. A PR-550 broadband polarization rotator (Newport Corp., Irvine, CA, USA) was used to rotate the polarization of the incident laser source, denoted by S and P polarizations. All spectra were processed and figures were prepared with Spectra-Solve for Windows software (LasTek Pty. Ltd., Thebarton, SA, Australia). Spectra were obtained with the incident beam aligned both along and normal to the four-fold rotation axis of vesuvianite.

3. Results and Discussion

3.1. Synthesis

Crystals of the synthetic vesuvianite, $Ca_{19}Al_{13}Si_{18}O_{68}O_3(OH)_7$ (**I**), were co-crystallized with synthetic grossular, $Ca_3Al_2(SiO_4)_3$, from the hydrothermal reaction of $CaSiO_3$ and Al_2O_3. The vesuvianite phase formed as elongated prismatic crystals (Figure 1, left) up to about 0.25 mm in length and were easily distinguishable from the rhombic dodecahedral grossular crystals. Powder X-ray diffraction confirmed the reaction product was a mixture of these two phases (Figure 2). The resulting grossular and vesuvianite crystals had similar sizes after the five-day reaction period, so it was not clear that one was necessarily the secondary product of the other. Crystals of **I** were obtained from various alkali hydroxide mineralizers, including 0.5 M NaOH, 0.1 M KOH, and 0.5 M RbOH. These mineralizers corresponded with much more highly basic solutions than were employed by Ito and Arem (pH 7–9.5), where Mg-free vesuvianite was not obtained under similar temperature

and pressure conditions [3]. Thus, it seems that the basicity of the solution may be a key reaction variable.

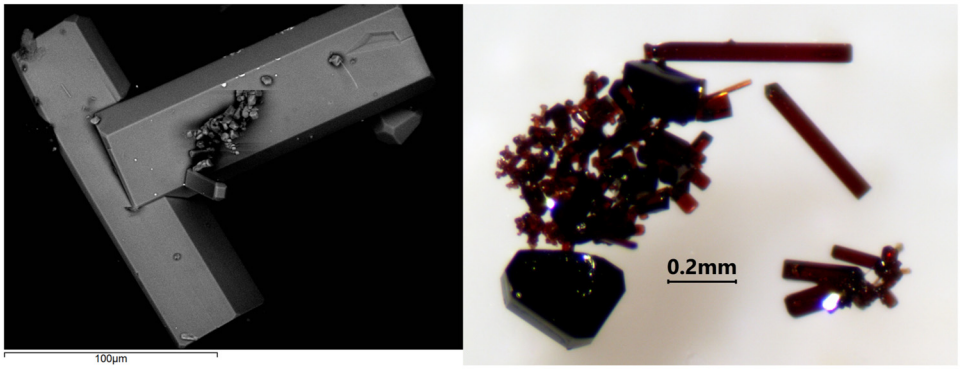

Figure 1. Left: electron micrograph of single crystals of the vesuvianite-type phase **I**. Right: optical micrograph of single crystals of the vesuvianite-type phase **II**.

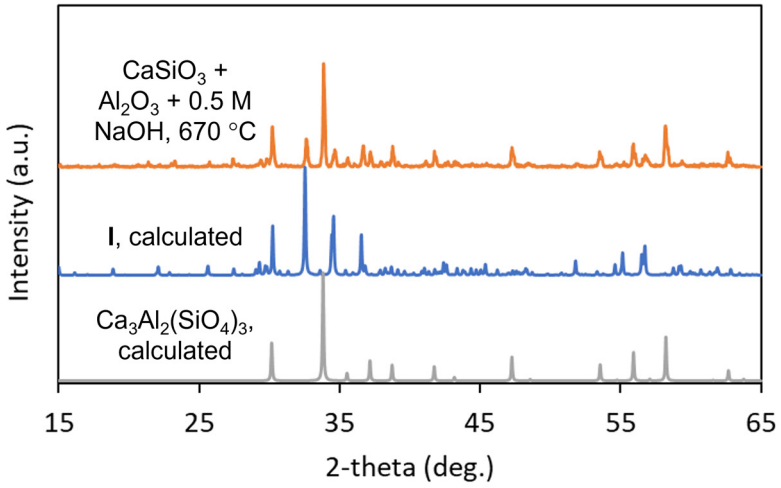

Figure 2. Powder X-ray diffraction pattern of the composite reaction product of $CaSiO_3$ + Al_2O_3 + 0.5 M NaOH at 670 °C, indicating a mixture of the vesuvianite-type phase, **I**, and grossular garnet phase $Ca_3Al_2(SiO_4)_3$.

The synthetic vesuvianite, $Sr_{19}Fe_{12}Ge_{19}O_{72}(OH)_6$ (**II**), formed as dark red crystals, both of columnar and block-like morphologies (Figure 1, right), with the color being indicative of the presence of Fe^{3+} ions in various relatively low site symmetries. The 3:1:3 reaction of SrO + Fe_2O_3 + GeO_2 used for the synthesis was nearly stoichiometric for the chemical formula of **II**, with respect to Sr:Fe:Ge. Powder X-ray diffraction confirmed that both the columnar and block-like morphologies corresponded to the germanate vesuvianite **II**, as the composite reaction products were found to contain only the vesuvianite phase (Figure 3). This was found to be the case for reactions involving both 3 M and 6 M alkali hydroxide mineralizers (NaOH, KOH, RbOH, CsOH) and the formation and crystal size was found to be independent of the identity of the alkali metal. Likewise, reactions that used Fe_2O_3 or FeO were both found to produce crystals of **II**. In the case of FeO, a molar ratio of 3:2:3 was used in the reaction of SrO + FeO + GeO_2 in 6 M KOH, also a nearly stoichiometric reaction for **II**. We saw several possible avenues to the in situ oxidation of Fe^{2+} of the feedstock to the Fe^{3+} state in the final product. One was the simple oxidation due to O_2 from the air in the sealed silver ampoules since we made no effort to exclude air when the ampoules were weld-sealed. The other could be the well-known stabilization of Fe^{3+} relative to Fe^{2+} in a strong aqueous base via $Fe^{2+} + OH^- \rightarrow Fe^{3+} + 1/2H_2 + O^{2-}$.

Ultimately, crystals of **II** formed in sizes up to 0.5 mm after seven days, from reactions utilizing Fe_2O_3 as the transition metal source and 6 M KOH as the mineralizer.

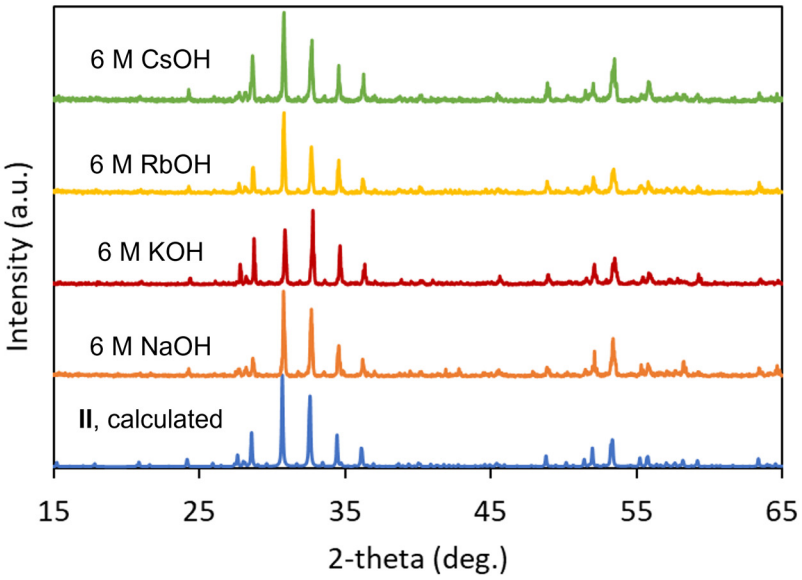

Figure 3. Powder X-ray diffraction patterns of the composite reaction products for reactions of 3 SrO + Fe_2O_3 + 3 GeO_2, indicating phase purity of the vesuvianite-type phase **II**.

3.2. Structural Analysis

3.2.1. Space Group Assignment

While the majority of natural vesuvianite has been refined in space group *P*4/*nnc*, subtle variations in the structure can lead the samples to crystallize in *P*4*nc* or *P*4/*n* with strong *P*4/*nnc* pseudosymmetry; these possibilities were well discussed in the previous literature [14–16]. Thus, we first sought to carefully evaluate the space group symmetry of the synthetic analogs **I** and **II**. While acentric *P*4*nc* vesuvianite can be verified through measurement of properties such as piezoelectricity or second-harmonic generation, *P*4/*n* vesuvianite cannot be easily distinguished from *P*4/*nnc*, other than through careful examination of the glide plane violating reflections in the diffraction data. Table 2 compares these glide plane violating reflections for the *P*4/*nnc* vesuvianite of this study (**I** and **II**), with one vesuvianite of each lower symmetry space group as previously presented by Armbruster and Gnos [16]. In evaluating the reflections corresponding to the *n*-glide perpendicular to the *c*-axis, (*n*--), it was clear that the lack of glide plane violating reflections in **I** and **II** was not consistent with space group *P*4*nc*, particularly when comparing the N I>3σ and <I/σ> values to those of the N'chwaning mine sample, which was shown to have *P*4*nc* symmetry. The (-*n*-) and (--*c*) classes of glide plane violating reflections can then be used to distinguish between *P*4/*nnc* and *P*4/*n*. The Asbestos mine sample shown to have *P*4/*n* symmetry had, by proportion, about 1.6–1.8 times more glide plane violating reflections for these classes than **I** and these reflections in **I** were much weaker, having nearly half of the <I/σ> values of those in the Asbestos mine sample. The proportions of N I > 3σ and <I/σ> values for (-*n*-) and (--*c*) in **I** were quite similar to those in the N'chwaning mine sample, which indeed did contain the respective *n*- and *c*-glides (though again, not the *n*-glide derived from the (*n*--) class). In these ways, the diffraction data of **I** was consistent with *P*4/*nnc*. In the case of **II**, there were virtually no appreciable glide plane violating reflections for any of the (*n*--), (-*n*-), or (--*c*) classes, which was consistent with *P*4/*nnc*.

Table 2. Comparison of the systematic absence exceptions in the single-crystal X-ray diffraction reflections of *P*4/*nnc* $Ca_{19}Al_{13}Si_{18}O_{71}(OH)_7$ and $Sr_{19}Fe_{12}Ge_{19}O_{72}(OH)_6$, the *P*4*nc* vesuvianite from the N'chwaning II mine (Republic of South Africa), and the *P*4/*n* vesuvianite from the Asbestos mine (Quebec) [16]. N = number of candidate reflections that should be systematically absent, N I > 3σ = number of candidate reflections having I/σ values greater than 3, <I> = average intensity of candidate reflections, <I/σ> = average intensity/uncertainty of candidate reflections.

	$Ca_{19}Al_{13}Si_{18}O_{71}(OH)_7$ ***P*4/*nnc***			**$Sr_{19}Fe_{12}Ge_{19}O_{72}(OH)_6$** ***P*4/*nnc***			**N'chwaning** ***P*4*nc***			**Asbestos** ***P*4/*n***		
Symmetry	*n*--	*-n-*	*--c*	*n*--	*-n-*	*--c*	*n*--	*-n-*	*--c*	*n*--	*-n-*	*--c*
N	332	624	375	1328	1828	1355	333	422	268	405	664	426
N I>3σ	5	141	98	1	39	13	140	125	68	5	270	177
<I>	0.1	0.4	0.5	0.3	0.4	0.4	1.1	0.7	0.7	0.2	1.5	1.5
<I/σ>	0.6	2.1	2.4	0.5	0.8	0.7	3.0	2.1	2.1	0.9	4.1	4.6

As further support of the space group assignment for **I**, we evaluated the single crystal Raman spectra (Figure 4). The spectra were consistent with vesuvianite having *P*4/*nnc* symmetry, most notably in the absence of an intense band around 640 cm^{-} that is characteristic of *P*4/*n* and other low-temperature ordered vesuvianite [27,28]. This was not unreasonable, as our material was prepared at a significantly higher temperature (670 °C) than those reported previously. A somewhat broad feature was present from 750 to 790 cm^{-} in the spectra taken normal to the four-fold rotation axis that was not present in the spectra obtained along the four-fold rotation axis. In general, there were only minor intensity changes in the bands that occurred with regards to the incident polarization.

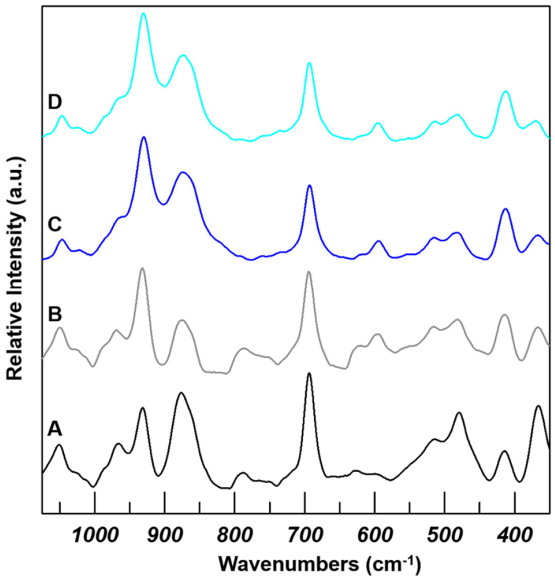

Figure 4. Single-crystal Raman spectra normal to the four-fold axis of vesuvianite (A—P-polarized, B—S-polarized) and along the four-fold axis of vesuvianite (C—P-polarized, D—S-polarized).

Finally, a series of test refinements were performed on the diffraction data of **I** and **II**, testing the quality of the models in *P*4*nc* and *P*4/*n*. In these test cases, the residual R1 values increased by about 0.005–0.01 compared with refinement in *P*4/*nnc*. Importantly, the *P*4*nc* and *P*4/*n* test refinements also resulted in significantly less favorable displacement parameters for the atoms, including numerous atoms with non-positive definite anisotropic displacement parameters. Refinement in *P*4/*nnc* was much more favorable in this respect, with all atoms exhibiting positive and reasonable displacement parameters. Details of the test refinements are provided in the Supplementary Information.

3.2.2. Structural Features

For ease of structural comparison, the atomic site numbering scheme was derived from that of Groat and coworkers in their review of the crystal chemistry of natural vesuvianite samples [1]. The synthetic $Ca_{19}Al_{13}Si_{18}O_{68}O_3(OH)_7$ in space group *P*4/*nnc* contained identical crystallographic sites and symmetry to crystals having the ideal vesuvianite formula $X_{19}Y_{13}Z_{18}O_{68}W_{10}$, namely three unique Si (*Z*) sites, four unique Ca (*X*) sites, three unique Al (*Y*) sites, and eleven unique O (O, *W*) sites (Table 3). Of these sites, Ca4 and Al1 were half-occupied in a channel, due to geometric considerations and consistent with the natural samples, which corresponded to a formula of $Ca_{19}Al_{13}(Si_2O_7)_4(SiO_4)_{10}O_3(OH)_7$. The synthetic $Sr_{19}Fe_{12}Ge_{19}O_{72}(OH)_6$ **II** was also solved in the space group *P*4/*nnc*; the sites in **II** were also consistent with the ideal vesuvianite formula, with four unique Ge (*Z*, *Y1*) sites, four unique Sr (*X*) sites, two unique Fe (*Y2*/*Y3*) sites, and eleven unique O (O, *W*) sites (Table 4), leading to a structural formula of $Sr_{19}Fe_{12}Ge(Ge_2O_7)_4(GeO_4)_{10}O_4(OH)_6$. In this case, the complex disorder within the channels often observed in the vesuvianite structure type was displayed via multi-site disorder within the channel, where Ge4 and Sr4 were both split into two sub-sites, Ge4a/Ge4b and Sr4a/Sr4b, with the combination of the site occupancies of each site adding up to 50% Ge and 50% Sr in the channel (an overall identical content to the Ca and Al channel contents in **I**).

Table 3. Positional and displacement parameters for $Ca_{19}Al_{13}Si_{18}O_{71}(OH)_7$ (**I**).

Site	Atom	x/a	y/b	z/c	Ueq (Å^2)	sof
X1	Ca1	0.250000	0.750000	0.750000	0.0089(2)	1
X2	Ca2	0.68930(4)	0.45589(4)	0.62048(5)	0.00824(12)	1
X3	Ca3	0.39865(5)	0.31832(5)	0.88814(7)	0.01636(15)	1
X4	Ca4	0.750000	0.750000	0.6500(2)	0.0107(4)	0.5
Y1	Al1	0.750000	0.750000	0.5350(4)	0.0118(6)	0.5
Y2	Al2	0.500000	0.500000	0.500000	0.0069(2)	1
Y3	Al3	0.37885(6)	0.61264(6)	0.62594(8)	0.00720(16)	1
Z1	Si1	0.250000	0.750000	0.500000	0.0060(3)	1
Z2	Si2	0.31920(6)	0.54145(6)	0.87110(7)	0.00617(15)	1
Z3	Si3	0.58384(6)	0.65099(6)	0.63484(7)	0.00760(15)	1
O1	O1	0.32742(14)	0.71949(15)	0.58569(19)	0.0082(4)	1
O2	O2	0.34061(15)	0.61747(15)	0.77819(19)	0.0093(4)	1
O3	O3	0.22184(14)	0.54881(15)	0.92346(19)	0.0085(4)	1
O4	O4	0.39337(14)	0.56251(15)	0.97038(19)	0.0087(4)	1
O5	O5	0.48577(16)	0.67069(15)	0.6775(2)	0.0113(4)	1
O6	O6	0.62081(18)	0.72815(16)	0.5592(2)	0.0179(5)	1
O7	O7	0.32773(15)	0.44477(15)	0.8219(2)	0.0118(4)	1
O8	O8	0.59127(14)	0.56069(14)	0.56660(19)	0.0089(4)	1
O9	O9	0.64494(14)	0.64494(14)	0.750000	0.0105(5)	1
O10	O10	0.750000	0.750000	0.3672(5)	0.0191(9)	1
H10	H10	0.750000	0.750000	0.2900(19)	0.050	0.5
O11	O11	0.43844(15)	0.50514(15)	0.63642(19)	0.0094(4)	1
H11	H11	0.457(7)	0.474(6)	0.715(7)	0.08(3)	0.75

The resulting structures are shown in Figure 5. Prominent features of the vesuvianite structure were the characteristic channels propagating along the *c*-axis that were bound by the well-ordered aluminosilicate framework in **I** or the iron germanate framework in **II**. In **I**, one channel contained alternating SiO_4 and CaO_8 units and this is often considered as part of the calcium aluminosilicate framework. Similarly, this channel was occupied by alternating GeO_4 and SrO_8 units in **II**. The other channel contained alternating AlO_5 and CaO_8 units and alternating GeO_5 and SrO_8 units in **I** and **II**, respectively (Figure 6). This second channel also contained a hydrogen bonding connection (O10-H10---O10), as discussed below. The long-range ordering of the building blocks in this channel has been shown to be the source of the variation in space groups, including *P*4/*n* and *P*4*nc*, in the various natural vesuvianite samples (see also Supporting Information, Figure S1) [15,16]. Crystals in those space groups were also associated with lower formation temperatures [15]. The crystals of the present study were prepared in the thermal regime where space group *P*4/*nnc* appeared to be the most stable structure type; the X-ray data were refined as such.

Test refinements for **I** were performed, where the occupancies of the *X*4 (Ca4) and *Y*1 (Al1) sites were allowed to freely refine, since the occupancy of these sites was integral in defining vesuvianite symmetry. The occupancies freely refined to 51.1% for Al1 and 48.7% for Ca4, supporting the occupancy pattern in *P*4/*nnc*. A similar free refinement was performed for **II**, but it was found that utilizing only two half-occupied sites in the channel was insufficient to account for the excess electron density between Sr4 and Ge4, so the sites were split further and given sub-half occupancy (Sr4a, Sr4b, Ge4a, and Ge4b). The free variable refinement was then used to determine the occupancy of each site; it was found that Sr4a and Ge4b were ~20% occupied and Sr4b and Ge4a were ~30% occupied.

Table 4. Positional and displacement parameters for $Sr_{19}Fe_{12}Ge_{19}O_{72}(OH)_6$ (**II**).

Site	Atom	x/a	y/b	z/c	Ueq (Å^2)	sof
X1	Sr1	0.250000	0.750000	0.250000	0.0033(2)	1
X2	Sr2	0.45670(3)	0.80989(3)	0.61902(5)	0.00307(12)	1
X3	Sr3	0.67853(4)	0.60061(4)	0.38584(5)	0.00668(13)	1
X4a	Sr4a	0.750000	0.750000	0.652(5)	0.0094(14)	0.2
X4b	Sr4b	0.750000	0.750000	0.650(3)	0.0084(10)	0.3
Y1a	Ge4a	0.750000	0.750000	0.5316(5)	0.0113(9)	0.3
Y1b	Ge4b	0.750000	0.750000	0.5936(10)	0.0132(13)	0.2
Y2	Fe2	0.500000	1.000000	0.500000	0.0052(2)	1
Y3	Fe3	0.38831(5)	0.87928(5)	0.37237(8)	0.00393(17)	1
Z1	Ge1	0.250000	0.750000	0.500000	0.0054(3)	1
Z2	Ge2	0.45893(4)	0.68107(4)	0.36976(5)	0.00250(13)	1
Z3	Ge3	0.65076(4)	0.91725(4)	0.63439(5)	0.00414(14)	1
O1	O1	0.2811(3)	0.8297(3)	0.4128(4)	0.0027(8)	1
O2	O2	0.3793(3)	0.6592(3)	0.2776(4)	0.0041(9)	1
O3	O3	0.4504(3)	0.7807(3)	0.4218(4)	0.0050(9)	1
O4	O4	0.4374(3)	0.6071(3)	0.4723(3)	0.0031(9)	1
O5	O5	0.6690(3)	1.0164(3)	0.6815(4)	0.0068(9)	1
O6	O6	0.7312(3)	0.8823(3)	0.5571(4)	0.0133(11)	1
O7	O7	0.5566(3)	0.6748(3)	0.3192(4)	0.0059(9)	1
O8	O8	0.5606(3)	0.9073(3)	0.5627(4)	0.0049(9)	1
O9	O9	0.6473(3)	0.8527(3)	0.750000	0.0073(12)	1
O10	O10	0.750000	0.750000	0.3676(12)	0.026(3)	1
H10	H10	0.750000	0.750000	0.28(4)	0.050	0.5
O11	O11	0.4942(3)	0.9381(3)	0.3622(3)	0.0043(8)	1
H11	H11	0.497800	0.969600	0.303400	0.050	0.625

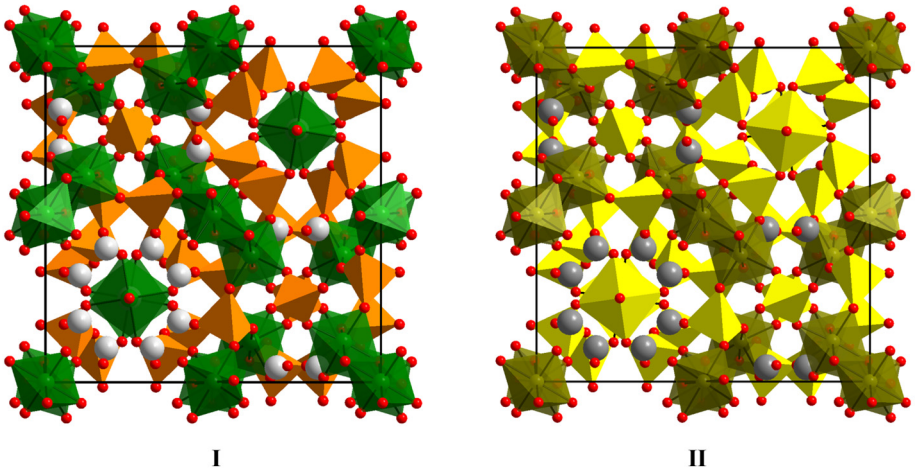

I **II**

Figure 5. Structure of $Ca_{19}Al_{13}Si_{18}O_{68}O_3(OH)_7$ (**I**, left) and $Sr_{19}Fe_{12}Ge_{19}O_{72}(OH)_6$ (**II**, right) along (001). Hydrogen atoms, as well as bonds to Ca2 and Ca3 (**I**) and Sr2 and Sr3 (**II**), are omitted for clarity. The color scheme is: orange = Si, forest green = Al, light gray = Ca, dark gray = Sr, yellow = Ge, moss green = Fe, red = O.

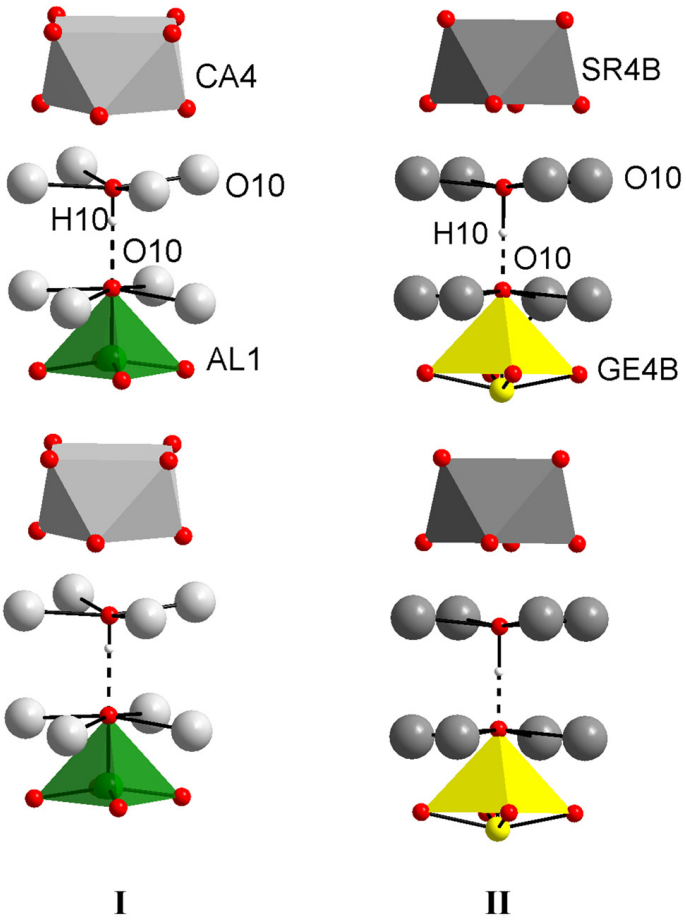

Figure 6. Channel contents Ca4, Al1, O10, and H10 in $Ca_{19}Al_{13}Si_{18}O_{68}O_3(OH)_7$ (**I**, left) viewed off (010). Additional Ca3 atoms bordering the channel are shown as green spheres to complete the geometry of O10. Likewise, additional O6 and O9 atoms bordering the channel are shown as red spheres to complete the geometries of Al1 and Ca4. In $Sr_{19}Fe_{12}Ge_{19}O_{72}(OH)_6$ (**II**, right), the Al1 site is replaced by Ge4a/Ge4b and the Ca4 atom is replaced by Sr4a/Sr4b.

Given the vast range of chemistry and substitutional behavior observed in natural vesuvianite, the $Ca_{19}Al_{13}Si_{18}O_{68}O_3(OH)_7$ and $Sr_{19}Fe_{12}Ge_{19}O_{72}(OH)_6$ formulas were corroborated using EDX, verifying the presence of only Ca, Al, Si, and O for **I** and Sr, Fe, Ge, and O for **II**. This was particularly useful in ruling out Na substitution as a mechanism for charge balance in **I**, since Na was present in the mineralizer solution. On a semi-quantitative metals basis, the relative elemental ratios in atomic percent for **I** (26.4% Al, 35.8% Si, and 37.7% Ca), as detected by EDX, compared favorably with those in the chemical formula of the single crystal structural model (26% Al, 36% Si, and 38% Ca). The relative elemental ratios of metals in **II** detected by EDX (29.9% Fe, 34.1% Ge, 36.0% Sr) differed only slightly from those based on the structural model (24% Fe, 38% Ge, 38% Sr). These synthetic formulas greatly simplified the exceedingly complex substitutional chemistry observed in the natural systems, as many of the natural specimens possess lanthanide ions, Fe^{3+}, Fe^{2+}, Ti^{4+}, Na^{+}, Cu^{2+}, Zn^{2+}, Mn^{2+}, B^{3+}, and F^{-} in significant quantities [8,9,29].

The controlled synthetic approach described here led to complete occupancy of Al^{3+} at the *Y* sites in **I** and complete occupancy of Ge^{4+} at the *Y1* site and Fe^{3+} at the *Y2* and *Y3* sites of **II**, with concomitant partial occupancy of the appropriate number of H^{+} ions from the OH sites in order to achieve charge balance. This behavior of the trivalent ions in the *Y* sites is interesting. The *Y* sites contributed 13 atoms to the formula unit in a fully occupied material, as observed here in $Ca_{19}Al_{13}Si_{18}O_{68}O_3(OH)_7$ and $Sr_{19}Fe_{12}Ge_{19}O_{72}(OH)_6$. Most natural samples typically contain between 8 and 11 aluminum atoms per formula unit. This

occurs since the half-occupied square pyramidal *Y*1 site can support a number of divalent and trivalent metal ions in natural samples and the *Y*1 site is often aluminum deficient or is substituted by divalent ions such as Fe^{2+} and Mg^{2+} [30]. Substitution of other common transition metals such as Fe^{3+} and Ti^{4+} at the *Y*2 and *Y*3 sites also contributes to lower aluminum contents in natural samples [1,12,31]. The full 13 aluminum atoms per formula unit were observed in **I** and 12 iron atoms from the *Y*2 and *Y*3 sites with one germanium atom from the *Y*1 site in **II** constituted simplified crystal–chemical compositions from the synthetic systems.

One implication of the high Al^{3+}, Fe^{3+}, and Ge^{4+} content in **I** and **II** was that the *W* sites must become more oxide rich to maintain charge balance. This full occupancy by the trivalent/tetravalent ions thus caused the corresponding decrease in OH^- stoichiometry in the final formula from typical values of approximately 10 in natural samples $X_{19}Y_{13}Z_{18}O_{68}(OH)_{10}$ to the synthetic analogs $X_{19}Y_{13}Z_{18}O_{78-x}(OH)_x$), where x = 7 and 6 for **I** and **II,** respectively. The ten *W* atoms per formula unit resided at two sites: O10 and O11. Both of these oxygen atoms were underbonded (Tables 5 and 6) with respect to their bond valence sums and both were shown to support hydrogen atoms to mitigate that deficiency [32]. The absence of fluorine in the synthetic samples also necessitated that both O10 and O11 sites be identified as O/OH in both compounds. Indeed, residual electron density corresponding to probable hydrogen atoms was observed around both of these atoms in our diffraction data and assigned as such. The position of H10 corresponded to that observed by Lager and coworkers using neutron diffraction and was half-occupied based on geometrical considerations [32]. The O10 site thus contributed one each of O and OH to the formula unit and a hydrogen bond connected O10 atoms within the channel. This left the O11 site to account for the remaining two O and six OH of the *W* formula units in **I** and three O and five OH of the *W* formula units in **II**. Thus, the hydrogen atom assigned to this site was $\frac{3}{4}$ occupied in **I** and 5/8 occupied in **II** and again occupied a comparable position to that traditionally assigned in vesuvianite and confirmed by Lager et al. The hydrogen atom occupancies were of course not derived by refinement of the X-ray data but were dictated by charge balance requirements.

Table 5. Bond valence sum calculations for $Ca_{19}Al_{13}Si_{18}O_{71}(OH)_7$ (**I**) (non-hydrogen atoms only).

Atom	O1	O2	O3	O4	O5	O6	O7	O8	O9	O10	O11	Sum
Ca1	0.37 (x4→)	0.23 (x4→)										2.40
Ca2	0.25	0.29	0.32	0.28	0.38, 0.27			0.38				2.17
Ca3			0.27			0.25	0.32, 0.23, 0.19	0.18		0.20 (x4↓)	0.23	1.87
Ca4						0.40 (x4→)			0.18 (x4→)			2.32
Al1						0.31 (x4→)				0.37		1.61
Al2				0.41 (x2→)				0.50 (x2→)			0.50 (x2→)	2.82
Al3	0.46	0.47	0.42	0.31	0.37						0.45	2.48
Si1	0.95 (x4→)											3.80
Si2		0.94	0.96	0.87			1.02					3.79
Si3					0.97	1.06		1.00	0.90 (x2↓)			3.93
Sum	2.03	1.93	1.97	1.87	1.99	2.02	1.76	2.06	1.98	1.17	1.18	

Table 6. Bond valence sum calculations for $Sr_{19}Fe_{12}Ge_{19}O_{72}(OH)_6$ (**II**) (non-hydrogen atoms only).

Atom	O1	O2	O3	O4	O5	O6	O7	O8	O9	O10	O11	Sum
Sr1	0.38 (x4→)				0.26 (x4→)							2.56
Sr2	0.27	0.30	0.35	0.27	0.37, 0.31			0.41				2.28
Sr3			0.27			0.26	0.37, 0.24, 0.23	0.21		0.19 (x4↓)	0.26	2.03
Sr4a						0.37 (x4→)			0.22 (x4→)			2.36
Sr4b						0.37 (x4→)			0.21 (x4→)			2.32
Ge4a						0.28 (x4→)				0.43		1.55
Ge4b						0.26 (x4→)						1.04
Fe2				0.43 (x2→)				0.55 (x2→)			0.52 (x2→)	3.00
Fe3	0.51	0.55	0.50	0.34	0.43						0.52	2.85
Ge1	0.92 (x4→)											3.68
Ge2		0.91	0.95	0.87			1.05					3.78
Ge3					0.97	1.04		1.02	0.88 (x2↓)			3.91
Sum	2.08	1.76	2.07	2.18	2.34	2.58	1.89	2.19	2.19	1.19	1.30	

The synthetic sample $Ca_{19}Al_{13}Si_{18}O_{68}O_3(OH)_7$ also provided baseline values for interatomic distances in the vesuvianite structural units (Table 7). Of particular interest was the *Y*1 site fully occupied by Al^{3+} in the present study. The Al1 site exhibited Al-O bond lengths of 1.977(6) and 2.057(2) Å. This was consistent with the smaller Al^{3+} in the synthetic vesuvianite compared with other vesuvianites, where the *Y*1 site was primarily assigned to other larger metal ions such as Fe^{2+} (Fe-O = 2.278 Å and 2.087 Å [30]; 2.267(5) Å and 2.080(1) Å [8]), Mn^{2+} (Mn-O = 2.04(4) Å and 2.051(4) Å) [9], and Fe^{3+} (Fe-O = 2.214(8) Å and 2.085(2) Å) [10]. One exception to this trend was that reported for Mg^{2+} (1.908(19) Å and 2.052(8) Å) [33]. Given the Shannon crystal radii of five-coordinate Mg^{2+} (0.66 Å) compared with the other common occupants of the *Y*1 site (for example, Fe^{3+} at 0.58 Å), it would appear the reported Mg-O10 distance was somewhat of an outlier and Al^{3+} (0.48 Å) obeyed the trend established by all of the other common *Y*1 site occupants [34]. The *Y*1-O differences were especially pronounced in the *Y*1-O10 interactions, since these were not constrained by the silicate framework and displayed more of a dependence on the composition of the *Y*1 site. The present synthetic sample **I,** with only Al^{3+} at the *Y*1 site, clearly exhibited a much shorter bond distance to O10, as would be expected from the absence of divalent ions at the site. Importantly, this *Y*1-O10 distance has also been shown to have correlations with the space group symmetry in vesuvianite, where non-*P*4/*nnc* materials exhibit *Y*-O10 bond lengths below 1.9 Å while still maintaining O10-O10 distances over 2.75 Å. In **I**, the Al1-O10 distance (1.977(6) Å) was clearly above this threshold, providing additional support for *P*4/*nnc* assignment. As a whole, the *Y*1 site was somewhat underbonded as Al^{3+}, which suggests that Al^{3+} was actually rather small for this site. This explains why the natural samples often had a larger divalent transition metal, or Mg^{2+} as the primary *Y*1 site occupant [1], though the presence of Al^{3+} was known to occur at the site, of course [35]. The lack of any reasonable alternative divalent occupant in the closed system of these synthetic experiments, which might otherwise be present in most natural systems, was likely what caused Al^{3+} to occupy the site in full. The unit cell parameters for this synthetic vesuvianite were within the expected range for non-boron-bearing vesuvianite observed in the comprehensive study by Groat et al. [1].

Table 7. Selected interatomic distances (Å) in $Ca_{19}Al_{13}Si_{18}O_{68}O_3(OH)_7$.

Bond	Length	Bond	Length
Ca1-O1 (x4)	2.3338(19)	Al1-O10	1.977(6)
Ca1-O2 (x4)	2.5168(19)	Al1-O6 (x4)	2.057(2)
Ca2-O8	2.3202(19)	Al2-O11 (x2)	1.877(19)
Ca2-O5	2.326(2)	Al2-O8 (x2)	1.8760(19)
Ca2-O3	2.384(2)	Al2-O4 (x2)	1.9539(19)
Ca2-O2	2.426(2)		
Ca2-O4	2.445(2)	Al3-O2	1.898(2)
Ca2-O5	2.450(2)	Al3-O1	1.902(2)
Ca2-O1	2.484(2)	Al3-O11	1.914(2)
		Al3-O3	1.942(2)
Ca3-O7	2.385(2)	Al3-O5	1.984(2)
Ca3-O3	2.453(2)	Al3-O4	2.054(2)
Ca3-O6	2.478(3)		
Ca3-O7	2.505(2)	Si1-O1 (x4)	1.6438(18)
Ca3-O11	2.512(2)		
Ca3-O10	2.5550(8)	Si2-O7	1.617(2)
Ca3-O7	2.588(3)	Si2-O3	1.639(2)
Ca3-O8	2.612(2)	Si2-O2	1.647(2)
		Si2-O4	1.677(2)
Ca4-O6 (x4)	2.304(3)		
Ca4-O9 (x4)	2.592(3)	Si3-O6	1.603(3)
		Si3-O8	1.623(2)
		Si3-O5	1.636(2)
		Si3-O9	1.6634(12)

The synthetic material $Sr_{19}Fe_{12}Ge_{19}O_{72}(OH)_6$ **II** provided an unusual example of a vesuvianite structure type enabled by synthetic substitutions. The lattice parameters were increased from the presence of the larger ions, with Sr^{2+} replacing Ca^{2+}, Fe^{3+} replacing Al^{3+}, and Ge^{4+} replacing Si^{4+} and Al^{3+}. We postulated that the substitution of the larger Fe^{3+} and Ge^{4+} ions into the *Y*2/*Y*3 and *Z* sites, respectively, assembled into a significantly larger iron germanate framework compared with the aluminum silicate framework, thus enabling the structure to support the larger Sr^{2+} (versus Ca^{2+}) cations (Table 8). Indeed, the Fe-O bond lengths at the *Y*2 and *Y*3 sites (averaging 2.017 Å at *Y*2 and 2.038 Å at *Y*3) were longer than those in the iron-rich natural vesuvianite (averaging 1.913 Å at *Y*2 and 2.018 Å at *Y*3) [8] due to the full Fe^{3+} occupancy in **II**. The Ge-O bond lengths of the *Z* sites of **II** were typical for Ge^{4+} and, thus, also contributed to the expanded lattice compared with silicate vesuvianites. Similar to Al1 in **I**, the *Y*1 sites (here occupied by disordered Ge4a/Ge4b) were significantly underbonded, indicating that, with the increased lattice size from the transition from a silicate to a germanate, the Ge^{4+} ion may similarly be a small ion for this site despite having a greater radius than Al^{3+}. It is possible that substitution of Ge^{4+} for a larger tetravalent or trivalent ion would make a more suitable alternative in controlled hydrothermal experiments and allow for less disorder within the channels. The EDS measurements suggested that the formula was stoichiometrically accurate, with ideal occupancy of the *X*, *Y*, and *Z* sites as expected, especially given the large differences in ionic size of the three ions. In this material, the two unique *Y* sites that were occupied by Fe^{3+} were six-coordinate, though relatively low in their site symmetries, enabling a considerable number of allowed electronic transitions, which explains the dark red color. Bond valence sums were likewise supportive of Fe^{3+} (Table 6). The presence of a different number of occupancies on each of the crystallographic sites would also suggest the possibility of ferrite (ferrimagnetic) type behavior. Magnetic studies will be the subject of a future publication.

Table 8. Selected interatomic distances (Å) in $Sr_{19}Fe_{12}Ge_{19}O_{72}(OH)_6$.

Bond	Length	Bond	Length
Sr1-O1 (x4)	2.471(4)	Sr4b-O6 (x4)	2.49(2)
Sr1-O5 (x4)	2.621(4)	Sr4b-O9 (x4)	2.69(2)
Sr2-O8	2.446(4)	Ge4b-O6 (x4)	2.245(6)
Sr2-O5	2.485(5)		
Sr2-O3	2.509(5)	Fe2-O8 (x2)	1.982(5)
Sr2-O2	2.569(5)	Fe2-O11 (x2)	2.000(4)
Sr2-O4	2.607(4)	Fe2-O4 (x2)	2.070(4)
Sr2-O5	2.551(5)		
Sr2-O1	2.601(4)	Fe3-O2	1.981(5)
Sr2-O6	3.048(5)	Fe3-O11	1.997(5)
		Fe3-O1	2.007(5)
Sr3-O7	2.490(5)	Fe3-O3	2.013(5)
Sr3-O3	2.598(5)	Fe3-O5	2.070(5)
Sr3-O6	2.617(5)	Fe3-O4	2.163(5)
Sr3-O7	2.652(5)		
Sr3-O11	2.614(4)	Ge1-O1 (x4)	1.779(4)
Sr3-O10	2.7338(14)		
Sr3-O7	2.660(5)	Ge2-O7	1.729(5)
Sr3-O8	2.701(5)	Ge2-O3	1.769(5)
Sr3-O6	3.190(5)	Ge2-O2	1.780(4)
		Ge2-O4	1.801(4)
Sr4a-O6 (x4)	2.49(3)		
Sr4a-O9 (x4)	2.69(3)	Ge3-O6	1.735(5)
		Ge3-O8	1.740(4)
Ge4a-O10	2.046(16)	Ge3-O5	1.760(5)
Ge4a-O6 (x4)	2.221(6)	Ge3-O9	1.792(3)

4. Conclusions

Vesuvianite serves as an interesting case study for the broader concept of emulating mineral crystal growth in the laboratory. It has a complex structure and a tremendously convoluted substitution chemistry among the natural samples. The synthesis of "clean" unsubstituted samples in the laboratory can help lead to an understanding of the conditions of phase formation as well as synthesizing foundational compositions that can be useful in characterizing the baseline structural or physical properties. This study of vesuvianite-types $Ca_{19}Al_{13}Si_{18}O_{68}O_3(OH)_7$ and $Sr_{19}Fe_{12}Ge_{19}O_{72}(OH)_6$ demonstrates that minerals exhibiting complex crystal chemistry and substitutional behavior can not only be prepared without substitutional impurities but can also be synthesized as simplified end members under carefully controlled synthetic conditions. In the present case, all sites host singular occupants and the structure is well refined with a minimum number of unique cations. Historically, the study of vesuvianite free of Mg, Fe, and other impurities has been surprisingly challenging, despite the wealth and variety of natural vesuvianite specimens. Compared with previous attempts to prepare synthetic vesuvianite, it appears that the greatly increased basicity of the mineralizer solution employed in the present study is important to the preparation of these crystals. This is another area where synthetic controls can be exploited, since reaction conditions (e.g., pH, temperature, and pressure) that may be less common in natural systems can be accessed synthetically. These controls over the chemistry and reaction conditions can be further extended to targeted compositions of minerals with interesting structures for subsequent structural or properties analysis. The work serves as an interesting case study of the convergence of synthetic hydrothermal chemistry and mineralogy and their cooperative study. Vesuvianite builds a case for the cooperative study of synthetic hydrothermal chemistry with other interesting mineralogical systems.

Supplementary Materials: The following supporting information can be downloaded at: https://www.mdpi.com/article/10.3390/cryst13081257/s1, Figure S1: Vesuvianite channel contents in

space groups *P*4/*n* and *P*4*nc*; Supplemental text: Additional details of test refinements of **I** and **II** for space group evaluation.

Author Contributions: Conceptualization, C.D.M. and J.W.K.; methodology, M.M.S. and C.A.M.; validation, M.M.S., C.A.M. and C.D.M.; formal analysis, M.M.S., C.A.M. and C.D.M.; investigation, M.M.S., C.A.M. and C.D.M.; writing—original draft preparation, C.A.M. and M.M.S.; writing—review and editing, C.D.M. and J.W.K.; visualization, C.A.M., M.M.S. and C.D.M.; funding acquisition, J.W.K. All authors have read and agreed to the published version of the manuscript.

Funding: This research was funded by National Science Foundation grants DMR-1410727 and DMR-2219129.

Data Availability Statement: CSD 2284129-2284130 contains the supplementary crystallographic data for this paper. These data can be obtained free of charge via http://www.ccdc.cam.ac.uk/conts/retrieving.html (or from the CCDC, 12 Union Road, Cambridge CB2 1EZ, UK; Fax: +44 1223 336033; E-mail: deposit@ccdc.cam.ac.uk).

Acknowledgments: The authors thank Daniel Willet and George Chumanov for assistance with the Raman spectra. We are likewise grateful for the contributions made by the anonymous reviewers toward improving the manuscript.

Conflicts of Interest: The authors declare no conflict of interest. The funders had no role in the design of the study; in the collection, analyses, or interpretation of data; in the writing of the manuscript; or in the decision to publish the results.

References

1. Groat, L.; Hawthorne, F.; Ercit, T.S. The Chemistry of Vesuvianite. *Can. Mineral.* **1992**, *30*, 19–48.
2. Allen, F.M.; Burnham, C.W. A Comprehensive Structure-Model for Vesuvianite; Symmetry Variations and Crystal Growth. *Can. Mineral.* **1992**, *30*, 1–18.
3. Ito, J.; Arem, J.E. Idocrase: Synthesis, Phase Relations and Crystal Chemistry. *Am. Mineral.* **1970**, *55*, 880–912.
4. Fitzgerald, S.; Leavens, P.B.; Nelen, J.A. Chemical Variation in Vesuvianite. *Mineral. Petrol.* **1992**, *46*, 163–178. [CrossRef]
5. Groat, L.; Hawthorne, F.; Ercit, T.S. Excess Y-Group Cations in the Crystal Structure of Vesuvianite. *Can. Mineral.* **1994**, *32*, 497–504.
6. Groat, L.A.; Hawthorne, F.C.; Ercit, T.S. The Incorporation of Boron into the Vesuvianite Structure. *Can. Mineral.* **1994**, *32*, 505–523.
7. Moiseev, M.M.; Panikorovskii, T.L.; Aksenov, S.M.; Mazur, A.S.; Mikhailova, J.A.; Yakovenchuk, V.N.; Bazai, A.V.; Ivanyuk, G.Y.; Agakhanov, A.A.; Shilovskikh, V.V.; et al. Insights into crystal chemistry of the vesuvianite-group: Manaevite-(Ce), a new mineral with complex mechanisms of its hydration. *Phys. Chem. Mineral.* **2020**, *47*, 18. [CrossRef]
8. Groat, L.A.; Evans, R.J.; Cempírek, J.; McCammon, C.; Houzar, S. Fe-rich and As-bearing vesuvianite and wiluite from Kozlov, Czech Republic. *Am. Mineral.* **2013**, *98*, 1330–1337. [CrossRef]
9. Groat, L.A.; Evans, R.J. Crystal Chemistry of Bi- and Mn-Bearing Vesuvianite from Langban, Sweden. *Am. Mineral.* **2012**, *97*, 1627–1634. [CrossRef]
10. Rucklidge, J.C.; Kocman, V.; Whitlow, S.H.; Gabe, E.J. The Crystal Structures of Three Canadian Vesuvianites. *Can. Mineral.* **1975**, *13*, 15–21.
11. Arem, J.E. *Crystal Chemistry and Structure of Idocrase*; Harvard University: Cambridge, MA, USA, 1970.
12. Groat, L.A. The Crystal Chemistry of Vesuvianite. Ph.D. Thesis, University of Manitoba, Winnipeg, MA, USA, 1988.
13. Allen, F.M. Structural and Chemical Variations of Vesuvianite. Ph.D. Thesis, Harvard University, Cambridge, MA, USA, 1985.
14. Groat, L.A.; Hawthorne, F.C.; Ercit, T.S.; Putnis, A. The Symmetry of Vesuvianite. *Can. Mineral.* **1993**, *31*, 617–635.
15. Gnos, E.; Armbruster, T. Relationship among Metamorphic Grade, Vesuvianite "Rod Polytypism", and Vesuvianite Composition. *Am. Mineral.* **2006**, *91*, 862–870. [CrossRef]
16. Armbruster, T.; Gnos, E. *P*4/*n* and *P*4*nc* Long-Range Ordering in Low-Temperature Vesuvianites. *Am. Mineral.* **2000**, *85*, 563–569. [CrossRef]
17. Panikorovskii, T.L.; Krivovichev, S.V.; Zolotarev, A.A.J.; Antonov, A.A. Crystal chemistry of low-symmetry (*P*4*nc*) vesuvianite from the Kharmankul' Cordon (South Urals, Russia). *Zap. Ross. Mineral. Obsh.* **2016**, *145*, 94–104.
18. McMillen, C.D.; Kolis, J.W. Hydrothermal Synthesis as a Route to Mineralogically-Inspired Structures. *Dalton Trans.* **2016**, *45*, 2772–2784. [CrossRef] [PubMed]
19. Sanjeewa, L.D.; McGuire, M.A.; Garlea, V.O.; Hu, L.; Chumanov, G.; McMillen, C.D.; Kolis, J.W. Hydrothermal Synthesis and Characterization of Brackebuschite-type Transition Metal Vanadate: $Ba_2M(VO_4)_2(OH)$, M = V^{3+}, Mn^{3+} and Fe^{3+} with Interesting Jahn Teller and Spin Liquid Behavior. *Inorg. Chem.* **2015**, *54*, 7014–7020. [CrossRef]
20. Sanjeewa, L.D.; Garlea, V.O.; McGuire, M.A.; McMillen, C.D.; Cao, H.; Kolis, J.W. Structural and magnetic characterization of the new one-dimensional S = 5/2 antiferromagnetic chain system $SrMn(VO_4)(OH)$. *Phys. Rev. B* **2016**, *93*, 224407. [CrossRef]

21. Terry, R.; McMillen, C.D.; Kolis, J.W. Hydrothermal Single Crystal Growth and Structural Investigation of the Nepheline and Kalsilite Stuffed Tridymite Species. *J. Chem. Crystallogr.* **2023**, *53*, 25–37. [CrossRef]
22. Warren, B.E.; Modell, D.I. The Structure of Vesuvianite $Ca_{10}Al_4(Mg,Fe)_2Si_9O_{10}(OH)_4$. *Z. Für Krist.-Cryst. Mater.* **1931**, *78*, 422–432. [CrossRef]
23. Smart, M.M.; Smith Pellizzeri, T.M.; Morrison, G.; McMillen, C.D.; zur Loye, H.-C.; Kolis, J.W. Ferrite Materials Containing Kagomé Layers: Chemistry of $Ba_2Fe_{11}Ge_2O_{22}$ and $K_2Co_4V_9O_{22}$ Hexaferrites. *Chem. Mater.* **2021**, *33*, 2258–2266. [CrossRef]
24. Smart, M.M.; McMillen, C.D.; Ivey, K.; Kolis, J.W. Chemistry of Transition Metal Silicates and Germanates: The Largest Metal Polygermanate, $K_{11}Mn_{21}Ge_{32}O_{86}(OH)_9(H_2O)$ with a 76 Å Ordered Lattice. *Inorg. Chem.* **2020**, *59*, 16804–16808. [CrossRef]
25. *Apex3 (version 2017.3)*; Bruker AXS Inc.: Madison, WI, USA, 2015.
26. Sheldrick, G.M. Crystal structure refinement with SHELXL. *Acta Crystallogr. Sect. C Struct. Chem.* **2015**, *71*, 3–8. [CrossRef]
27. Galuskin, E.; Galuskina, I.; Stadnicka, K.; Armbruster, T.; Kozanecki, M. The Crystal Structure of Si-Deficient, OH-Substituted, Boron-Bearing Vesuvianite from the Wiluy River, Sakha-Yakutia, Russia. *Can. Mineral.* **2007**, *45*, 239–248. [CrossRef]
28. Paluszkiewicz, C.; Żabiński, W. Vibrational Spectroscopy as a Tool for Discrimination of High and Low Vesuvianite. *Vib. Spectrosc.* **2004**, *35*, 77–80. [CrossRef]
29. Groat, L.A.; Hawthorne, F.C.; Ercit, T.S. The Role of Fluorine in Vesuvianite: A Crystal-Structure Study. *Can. Mineral.* **1992**, *30*, 1065–1075.
30. Ohkawa, N.; Yoshiasa, A.; Yakeno, S. Crystal Chemistry of Vesuvianite: Site Preferences of Square Pyramidal Coordinated Sites. *Am. Mineral.* **1992**, *77*, 945–953.
31. Panikorovskii, T.L.; Chukanov, N.V.; Rusakov, V.S.; Shilovskikh, V.V.; Mazur, A.S.; Balassone, G.; Ivanyuk, G.Y.; Krivovichev, S.V. Vesuvianite from the Somma-Vesuvius Complex: New Data and Revised Formula. *Minerals* **2017**, *7*, 248. [CrossRef]
32. Lager, G.A.; Xie, Q.; Ross, F.K.; Rossman, G.R.; Armbruster, T.; Rotella, F.J.; Shultz, A.J. Hydrogen-Atom Positions in *P*4/*nnc* Vesuvianite. *Can. Mineral.* **1999**, *37*, 763–768.
33. Valley, J.W.; Peacor, D.R.; Bowman, J.R.; Essene, E.J.; Allard, M.J. Crystal Chemistry of a Mg-Vesuvianite and Implications of Phase Equilibria in the System CaO-MgO-Al_2O_3 -SiO_2-H_2O-CO_2. *J. Metamorph. Geol.* **1985**, *3*, 137–153. [CrossRef]
34. Shannon, R.D. Revised Effective Ionic Radii and Systematic Studies of Interatomic Distances in Halides and Chalcogenides. *Acta Crystallogr. A* **1976**, *32*, 751–767. [CrossRef]
35. Phillips, B.L.; Allen, F.M.; Kirkpatrick, R.J. High-Resolution Solid-State ^{27}Al NMR Spectroscopy of Mg-Rich Vesuvianite. *Am. Mineral.* **1987**, *72*, 1190–1194.